PROBING THE BINDING SITES AND MECHANISMS OF ACTION OF

TWO hERG CHANNEL ACTIVATORS, NS1643 AND PD307243

Xulin Xu[1], Maurizio Recanatini[2], Marinella Roberti[2], Gea-Ny Tseng[1]

1. Department of Physiology

Virginia Commonwealth University

Richmond, VA

2. Department of Pharmaceutical Sciences

University of Bologna

Bologna, Italy

Running title: HERG activators, channel inactivation and selectivity filter

For correspondence:
Gea-Ny Tseng, PhD
Department of Physiology
Virginia Commonwealth University
1101 E. Marshall Street
Richmond, VA 23298
Phone: 804-827-0811
Fax: 804-828-7382
e-mail: gtseng@vcu.edu

Number of text pages: 40

Number of table(s):   1

Number of figures: 10

Number of references: 33

Number of words in the *Abstract*:   249

Number of words in the *Introduction*: 705

Number of words in the *Discussion*:   1495

Nonstandard abbreviations:

PD	=	PD307243
NS	=	NS1643
V_t	=	test pulse voltage
V_r	=	repolarization voltage
I_{f-a}	=	fully-activated current
-S-S-	=	disulfide bonded state
+MTS	=	treated by a methanethiosulfonate reagent
TPeA	=	tetrapentylammonium
DOF	=	dofetilide

ABSTRACT

We studied the mechanisms and sites of activator actions of PD(307243) and NS(1643) on the

hERG channel expressed in oocytes and COS-7 cells. PD and NS affected hERG in a

concentration-dependent manner, reaching a maximal increase in current amplitude by 100% and

$\geq$ 300% (1-s test pulse to 0 mV), with apparent K_d values of 3 and 20 uM, respectively. Both

drugs slowed hERG inactivation. NS additionally shifted the activation curve in the negative

direction, accelerated activation and slowed deactivation. Kinetic model simulations suggested

that the activator effects of PD and NS could be largely accounted for by their effects on the

hERG gating kinetics. Both drugs worked from outside the cell membrane but their binding sites

appeared to be distinctly different. Perturbing the conformation of outer vestibule/external pore

entrance (by cysteine substitution at high-impact positions or cysteine side chain modification at

intermediate-impact positions) prevented the activator effect of NS but not that of PD.

Furthermore, a peptide toxin BeKm-1 that bound to the outer mouth of the hERG channel

suppressed NS effect but potentiated PD effect. We propose that NS is a 'gating-modifier': it

binds to the outer vestibule/pore entrance of hERG and increases current amplitudes by

promoting channel activation while retarding inactivation. PD's activator effect was prevented by

external quaternary ammonium cations or dofetilide, which approached the hERG selectivity

filter from opposite sides of the membrane and depleted K^+ ions in the selectivity filter. We

suggest that PD may work as a 'pore-modifier' of the hERG channel.

INTRODUCTION

The *human ether-a-go-go related gene* encodes the pore-forming component of the rapid delayed rectifier (I_{Kr}) channel (Sanguinetti *et al.*, 1995). The hERG/I_{Kr} channel is important for action potential repolarization in the heart (Tseng, 2001). Mutations in hERG/I_{Kr} have been linked to congenital long QT (LQT2) or short QT (SQT1) syndrome (Brugada *et al.*, 2004). A more common problem is the sensitivity of hERG/I_{Kr} channel to a wide range of drugs (Recanatini *et al.*, 2005). Unintentional drug blockade of hERG/I_{Kr} is the major cause for the acquired LQT syndrome (aLQT) (Roden, 2004). This problem has prompted the development of 'hERG activators' to combat aLQT, and perhaps LQT2. To achieve this goal, the hERG activators should be able to increase currents through the channel under a wide range of conditions: channel blockade by different chemicals as seen in aLQT, and channel malfunction due to various mutations as seen in LQT2. To design such robust hERG activators, knowledge about the mechanisms and sites of actions of available hERG activators is important.

Three major classes of hERG channel activators are available, represented by the following prototypes: RPR260243 (Kang *et al.*, 2005), NS1643 (Casis *et al.*, 2006; Hansen *et al.*, 2006) and PD118057 (Zhou *et al.*, 2005). The mechanism and site of action of RPR260243 have been elucidated recently. RPR260243 slows hERG channel deactivation (Kang *et al.*, 2005). Mutations of specific residues in the S4-S5 linker, cytoplasmic halves of S5 and S6 could attenuate or abolish the activator effect of RPR260243 (Perry *et al.*, 2007). Mapping these positions to the Kv1.2 crystal structure showed that they are close to each other in 3-D space, in a region critically involved in the voltage-dependent activation/deactivation gating processes (Long *et al.*, 2005). These observations provided a satisfying explanation for the pharmacological action of RPR260243.

A previous study on NS1643 suggested that this hERG activator mainly increased outward, but not inward, currents through the channels (Casis *et al.*, 2006). Furthermore, mutations at the external pore entrance and in the pore loop that perturb the inactivation process of the hERG channel can attenuate the activator effect of NS1643. On the other hand, mutations of an aromatic residues (F656) on S6, that is critical for hERG blocker binding within the inner cavity (Kamiya *et al.*, 2006), potentiate the activator effect of NS1643 (Casis *et al.*, 2006). It was suggested that NS1643 works mainly by hindering channel inactivation. However, detailed analysis of the effects of NS1643 on hERG gating kinetics has been limited, so that the mechanism and site of its activator action are not entirely clear.

A previous study on PD118057 showed that this drug increased outward currents through the hERG channels with little effects on the voltage-dependence or kinetics of activation and deactivation (Zhou *et al.*, 2005). PD118057 also slowed the rate of channel inactivation at $36^{o}C$. A recent study on PD307243, a structure analog of PD118057, showed that this hERG activator could dramatically slow the rate of channel deactivation, to the extent that some of the channels became constitutively active at hyperpolarized voltages (Gordon *et al.*, 2008). The authors also reported that PD307243 greatly slowed the rate of hERG inactivation at depolarized voltages. A combination of these two effects created a transient outward current (I_{to})-like channel phenotype for the hERG channel (Gordon *et al.*, 2008). There have been no mutagenesis experiments to probe for the binding site of PD118057 or PD307243 in the hERG channel. The mechanism for the peculiar pharmacological actions of PD307243 is not clear.

We undertook the present study to investigate the mechanisms and sites of activator actions of PD307243 and NS1643 (chemical structures shown in Zhou *et al.*, 2005, and Casis *et al.*, 2006) . Experiments were designed to systematically address the following questions:

1. How do these drugs modify the gating kinetics of the hERG channel, and can the drug effects on channel gating account for their activator actions?

2. Is there a membrane 'sidedness' in the activators' actions? This information is needed for the design of the following experiments to probe for the drug binding sites.

3. How do perturbations of the outer vestibule and external pore entrance of the hERG channel impact on the activator actions of PD307243 and NS1643?

4. How do pore blockers from outside or inside the cell membrane impact on the activator actions of PD307243 and NS1643?

MATERIALS AND METHODS

1. **Molecular biology**

The hERG1 WT cDNA was a kind gift from Dr. Gail A. Robertson (Wisconsin University). The hERG cDNA was subcloned into a vector, pAlterMax, and site-specific cysteine (Cys) substitutions were made using the oligonucleotide-directed method and a commercial kit (Altered Site[R] Mammalian Mutagenesis System, Promega) as described in our previous publications (Liu *et al*., 2002). Mutations were confirmed by DNA sequencing. Transcription of cRNAs was performed using the Mmessage Mmachine kit from Ambion. The concentrations and quality of cRNA products were examined using cRNA gel densitometry (ChemiImager Model 4000, α-Innotech) before oocyte injection.

2. **Oocyte experiments**

Oocytes were isolated as described previously (Liu *et al*., 2002). Each oocyte was microinjected with 40 nl of cRNA solution (total cRNA 10 - 18 ng). After cRNA injection,

oocytes were incubated in ND96 medium (in mM: NaCl 96, KCl 2, CaCl$_2$ 1.8, MgCl$_2$ 1, HEPES 5, Na-pyruvate 2.5, pH 7.5) supplemented with horse serum (4%) and antibiotics (penicillin 50 U/ml and streptomycin 50 U/ml) for 3- 5 days before experiments. Voltage clamp was performed using the '2-cushion pipette' methods (Schreibmayer *et al.*, 1994). Oocytes were superfused or bathed in a low [Cl]-ND96 solution (Cl$^-$ ions in ND96 replaced by methanesulfonate, to minimize interference from oocyte endogenous Cl currents), and membrane currents were recorded using an Oocyte Clamp amplifier (model 725B or 725C, Warner Instruments). Voltage clamp protocol generation and data acquisition were controlled by pClamp 5.5 via computer and a 12-bit D/A and A/D converter (Axon Instruments).

3. COS-7 experiments

COS-7 cells were maintained in D-MEM (Gibco) supplemented with 10% fetal calf serum (Hyclone) and penicillin/streptomycin, in a moist 5% CO$_2$ chamber at 36°C. Cells were plated at a sub-confluence level the day before transfection. Each 35-mm dish was added cDNAs for hERG (1 ug) and CD8 (0.2 ug), reaching cDNA molar ratio of 1:0.25. Currents were recorded 24-48 hr after transfection. Cells were exposed to CD8 mAb-coated beads (Dynal) at room temperature for 10 min, treated with trypsin-EDTA (Gibco) at room temperature for 5 min, and cell suspension was added to a poly-L-lysine coated coverslip placed in the cell chamber. Cells decorated with CD8-mAb beads were used for patch clamping. The pipette solution contained (mM): K-aspartate 115, KCl 20, EGTA 10, ATP(K salt) 10, MgCl$_2$ 1, and HEPES 10 (pH 7.3). Pipette tip resistance was 1.9 - 2.1 MΩ, and 95% of series resistance was compensated. The bath solution was normal Tyrode's (mM): NaCl 147, KCl 4, CaCl$_2$ 2, MgCl$_2$ 1, HEPES 5, and dextrose 5.5 (pH 7.3). Whole cell patch clamp was performed using AxoPatch 200B

controlled by pClamp10 via DigiData1440A. Methods of data analysis were similar to those

described for oocyte experiments.

4. Guinea pig ventricular myocyte experiments

Myocytes were isolated from a young adult male guinea pig (375 g) using collagenase

digestion followed by gentle mechanical trituration as described before (Yao *et al.*, 1999). Whole

cell current recording conditions were similar to those described for COS-7 experiments, except:

(1) during current recording, myocytes were superfused with a nominally Na- and Ca-free

Tyrode's solution (NaCl and $CaCl_2$ replaced by equimolar choline-Cl and $MgCl_2$), and (2)

recoding temperature was 33-34°C. Guinea pig ventricular myocytes express a sizable I_{Kr} as well

as a robust slow delayed rectifier current (I_{Ks}) (Sanguinetti and Jurkiewicz, 1990). However, we

could not identify reagents or conditions that could selectively suppress I_{Ks} without affecting I_{Kr},

to allow a direct detection of agonist effects on I_{Kr}. Therefore, we relied on the difference in the

voltage range of activation between I_{Kr} and I_{Ks} (Sanguinetti and Jurkiewicz1990). At 33-34°C

the most suitable voltage range for recording I_{Kr} (as a time-dependent outward current largely

free of I_{Ks}) was -20 to -10 mV. Removing extracellular Na and Ca ions was necessary since this

voltage range overlapped with those of Na and Ca channel currents.

5. Data analysis and kinetic model simulations

The voltage clamp protocols and methods of data analysis used to characterize the effects

of PD307243 and NS1643 on voltage-dependence and rate of activation, deactivation and

inactivation of the hERG channel are described in Fig. 1 and legend. Simulations of hERG

gating kinetics and drug effects were based on a hERG gating model described previously (Wang *et al.*, 1997) using a computer program, ModelMaker4 (AP Benson Ltd).

6. **Drug solutions and application**

PD307243 and NS1643 were generous gift from Dr. Xiaoping Xu (GlaxoSmithKline). Their stock solutions (10 mM in DMSO) were divided into 100 ul aliquots, and stored at -20°C until experiments. On the day of experiments, an aliquot was thawed, kept on ice and protected from light during the course of the experiments. In early experiments, we applied these drugs using the superfusion (flow-bath) method. The stock solutions were added to the low-[Cl] ND96 to reach desired final concentrations and the oocytes were superfused with the drug-containing solutions. In most of the experiments reported here, we applied the drugs using a 'non-flow' bath method. The oocytes were placed in 0.8 ml of low-[Cl] ND96 without superfusion, and impaled with two electrodes. After obtaining the control data, PD307243 or NS1643 stock solution was mixed with 0.2 ml low-[Cl] ND96 (to reach the desired final concentration when diluted 5 fold) and added to the bath. The solution was mixed by gently pipetting the bath solution up-and-down. When using the non-flow bath method, the agar salt bridges connecting the 3 M KCl/Ag/AgCl grounding electrodes to the bath solution were made in 2 mM [K] to avoid leakage of K^{+} ions into the bath solution. There were no discernible differences in results from these two methods of drug application and the data were pooled.

Other drugs used in the experiments included: BeKm-1 (recombinant form, Alomone Lab, 200 uM stock in ND96 containing 0.5% BSA, diluted to 10 nM final concentration by adding 50 nl of the stock to 1 ml of bath solution containing 0.5% BSA; BSA served to prevent peptide from sticking to plastic surface), tetrapentylammonium Cl (Sigma-Aldrich, 1 M stock in

water, final concentration 50 uM) and dofetilide (a gift from Pfizer, 1 mM stock in water, pH 3, final concentration 0.5 uM).

In the experiments shown in Fig. 5, PD307243, NS1643 and TEA were injected into oocytes during the course of recording. The micro-dispenser injecting device was the same as that used for cRNA injection. Assuming an oocyte volume of 0.5 ul (sphere with 1 mm diameter), the following stock solutions and injection volumes were used to reach the estimated final cytoplasmic concentrations: PD307243 -15 nl of 10 mM stock to reach 300 uM, NS1643 - 20 nl of 25 mM stock to reach 1000 uM, and TEA - 20 nl of 50 mM stock to reach 2 mM.

7. **Chemical analysis of PD307243**

Because the effects of PD307243 on hERG reported here differed markedly from those reported previously (Gordon *et al*., 2008), we analyzed the chemical structure of PD307243 used in our experiments. ^{1}H-NMR and ^{13}C-NMR spectra were recorded at 300 MHz and at 75 MHz, respectively. Electronspray ionization (ESI) mass spectrum was performed on a Waters MZQ Micromass ZQ 4000. High resolution mass spectrum (HRMS) was recorded on a Thermo Finnigan Mat 95XP. Results are presented as *Supplemental Data*.

RESULTS

1. **PD307243 and NS1643 exerted 'activator' effects on the hERG channel and altered the channel's gating kinetics**

Figs. 1 and 2 illustrate detailed characterization of the effects of PD307243 and NS1643 (abbreviated as PD and NS in the following text) on the hERG channel expressed in oocytes. Both drugs increased the hERG current amplitude in a concentration-dependent manner (Figs.

1A and 2A). Such 'activator' effects were seen in both outward and inward currents (Figs. 1H and

2H). In most experiments, we used the test pulse current amplitude at 0 mV to quantify drugs'

activator effects (except data in Figs. 5 - 7, noted in the figures or legends). We wished to

compare the apparent binding affinity and potency of the activator effect between PD and NS.

Assuming that both activators bound to the hERG channel in a 1:1 stoichiometry, and activator

binding increased the current amplitude to 'A' fold of control, the drug-channel interaction could

be described by the scheme.

At equilibrium in the presence of activator concentration [D], $R = K_d/([D] + K_d)$, $R^* =$

$[D]/([D] + K_d)$. The ratio of current amplitude in the presence of activator (I_d) to control (I_c) will

be: $I_d/I_c = R + (R^*A)$. This leads to equation [1] describing the relationship between I_d/I_c and [D]:

$$I_d/I_c = 1 + (A - 1)/(1 + K_d/[D]) \qquad [1]$$

Because PD had a secondary current-suppressing effect on the hERG channel (that became more

apparent at concentrations ≥ 20 uM, or in the presence of pore blockers, see below), we fit the

concentration-response relationship for [PD] 1 - 10 uM. The 'A' value was 2, and K_d value was 3

uM (Fig. 1B). In some oocytes NS at concentrations ≥ 60 uM induced a membrane 'leak'

conductance (thus the large standard error bars at 60 and 90 uM in Fig. 2B). Nevertheless, we fit

the complete concentration-response relationship of NS (3 - 90 uM) with equation [1], and

obtained 'A' and K_d values of 3.24 and 20 uM, respectively. In the following experiments, we

used [PD] of 10 or 20 uM and [NS] of 30 uM, i.e. concentrations that could induce significant

effects on the hERG current amplitude without appreciable secondary current-suppressing or

leak-inducing effects.

Both activators slowed the inactivation rate of the hERG channel to ~ 50% of control,

without altering its voltage-sensitivity (Figs. 1G and 2G). However, the two differed in how they

influenced the activation/deactivation gating processes of the hERG channel. PD did not shift the

voltage-dependence of activation (measured by the 1-s isochronal activation curve, Fig. 1C). It

had no effect on the rate of hERG activation (measured by the 'envelope' voltage clamp protocol

shown in Fig. 1E), or the time course of deactivation (quantified by double-exponential curve

fitting, Fig. 1F). On the other hand, NS consistently shifted the 1-s isochronal activation curve in

the negative direction (by ~ 10 mV) and accelerated hERG activation (Fig. 2C and 2E). NS also

slowed the rate of hERG deactivation, manifested by a prolongation of the fast and slow time

constants (Fig. 2F), although the distribution of the 2 components at different voltages was not

affected (data not shown). PD and NS also differed in the voltage-dependence of their activator

effects on the test pulse current (measured by current ratio or I_d/I_c). While the value of I_d/I_c for

PD showed an increase with stronger depolarization (Fig. 1D), the opposite was seen with NS

(Fig. 2D).

2. **Could the activator effects of PD307243 and NS1643 be accounted for by their effects**
   on hERG channel gating kinetics?

      We used a kinetic model for hERG channel gating described previously (Wang *et al.*,

1997) to test whether the activator effect of PD on the hERG channel could be accounted for by

the drug-induced slowing of inactivation. The kinetic model and parameter values used in the

simulations are described in Table 1. The only change we made for PD was a 50% decrease in

the forward rate of channel inactivation, in accordance with the experimental data shown in Fig.

1: PD reduced the rate of hERG inactivation by 50% without changing its voltage-sensitivity, or

parameter values related to the activation/deactivation gating processes. The simulation results

are shown in Fig. 3A. The model could qualitatively mimic the effects of PD on hERG test pulse

currents (panels a and c), tail currents (a) and rate of inactivation (d). There was no shift in the

voltage-dependence of activation (b).

To check whether we could simulate the NS effects on the hERG channel, we made the

following changes in the model parameters: (1) forward rate constant of inactivation reduced by

50%, based on the slowing effect of NS on the rate of inactivation without altering the voltage-

sensitivity, (2) forward rate constant from C_2 to O states increased to 4 fold, and (3) backward

rate constant from O to C_2 decreased by 75%. We chose to modify the transition rates between

the O state and the immediate C_2 state based on the experimental data shown in Fig. 2F. The time

course of hERG channel deactivation could be described by a double exponential function in the

V_r range > -100 mV, but mainly a single (fast) exponential function in more negative V_r range.

The probable explanation for this kinetic behavior is that the fast deactivation component is

mainly due to the backward transition from the O state to the immediate closed state, while the

slow deactivation component is due to the residual forward transitions between closed states in

the less negative voltage range. Therefore, to be consistent with the finding that NS significantly

slowed the fast component of deactivation even at -120 mV, we altered the transition between O

and C_2 states. The amount of changes described above was needed to reproduce the negative

shift in the activation curve by -10 mV (Fig. 2C). The results of simulation of the NS effects are

shown in Fig. 3B. The model qualitatively mimicked the effects of NS on the test pulse current

(panels a and c), tail current (a), rate of inactivation (d) and voltage-dependence of activation (b).

Fig. 4 shows the concentration-response relationships of PD and NS on the hERG

channel. The data support the above notion that PD's agonist effect was accompanied mainly by

a slowing of hERG inactivation, while NS's agonist effect had contribution from both a slowing

of hERG inactivation and a stabilization of the channel in the activated vs closed states (denoted

by the negative shift in $V_{0.5}$ of activation). Model prediction of the agonist effects of PD and NS

appeared less than those observed experimentally (Figs. 1 and 2). Prolonged whole cell recording

was accompanied by a gradual run-up of the hERG current amplitudes (Fig. S1 in *Supplemental*

Data), that could cause an overestimation of the agonist effects.

The model-predicted relationship between 'V_t' and 'I_d/I_c' provided an explanation for the

experimental findings of opposite trends for PD vs NS (Fig. 1D and 2D). For the PD simulation,

the values of I_d/I_c gradually increased as the V_t became more depolarized, and plateaued at $V_t \geq$

+40 mV. This was due to the fact that the only change we introduced for PD in the hERG gating

model was a reduction in the forward transition rate from O to I states, which was voltage-

sensitive. As V_t became more depolarized, the rate of inactivation became a more dominating

factor in determining the current amplitude, and thus slowing it would cause a higher % of

increase in the current amplitude. For the NS simulation, the I_d/I_c value was highest at the

threshold depolarization voltage, and steadily declined as V_t became more depolarized,

approaching a steady level at $V_t \geq$ +20 mV. This was due to the fact that NS caused a more

prominent increase in channel open probability at more negative V_t (but above the threshold of

activation, panel b). This trend contributed to the higher I_d/I_c values from -60 to +20 mV. At

more positive V_t, slowing of inactivation was the main factor for the increase in current

amplitude, as in PD simulation, and I_d/I_c approached a similar value of ~2.

3. **Both PD307243 and NS1643 acted on the hERG channel from the extracellular side of**
   the cell membrane but their effects were additive

A prerequisite for the search of a drug's binding site in a membrane channel is to know

whether there is 'membrane sidedness' in the drug's actions, i.e. whether the drug is effective only

when applied from inside or outside the cell membrane. Once this information is available,

proper strategies can be designed (e.g. site-specific mutations, pharmacological or ionic

perturbations) to gain further insights into the channel domain(s) where the drug may bind. Figs.

1A and 2A show that the effects of PD and NS (applied by directly adding the drug solution to

the bath solution followed by pipetting up-and-down to mix the two, the 'non-flow' bath, see

Methods) had very rapid onset, and the activator effects could be seen in the low uM

concentration range. Importantly, the potency of PD tested in oocytes was not different from that

of PD tested in mammalian COS-7 cells (Figs. 5A vs 5B). If these activators worked on the

hERG channel from the intracellular side of the cell membrane, the yolk inside oocytes would

provide a huge sink for the lipophilic drug molecules, leading to a decrease in the apparent drug

potency and a delay in the onset of drug effects, as is the case for quinidine (Yeola *et al.*, 1996;

Zhang *et al.*, 1998). Since COS-7 cells do not have yolk, we expected to see much higher drug

potency when tested in the mammalian cells vs in oocytes. To check whether PD and NS worked

on the hERG channel from the extracellular side of the cell membrane, we directly compared the

potency of these drugs applied by intra-oocyte injection vs by bath application. Figs. 5B and 5C

show that intra-oocyte injection of a high concentration of PD (300 uM) or NS (1000 uM) had no

discernible effect on the hERG current amplitude or gating kinetics. However, subsequent bath

application of a 30-fold lower concentration of PD (10 uM) or NS (30 uM) effectively increased

the hERG current amplitude. To confirm the effectiveness of our intra-oocyte injection

technique, in both experiments we pulled out the injecting pipettes, expelled the remaining drug

solutions in the pipette tips, refilled the pipette tips with a TEA solution, reimpaled the oocytes

and injected ~ 20 nl of TEA solution into the oocytes (comparable to the volume of drug solution

injected). In both cases, intra-oocyte injection of TEA to reach an estimated cytoplasmic

concentration of 2 mM effectively suppressed the hERG current. These observations confirmed

that both PD and NS worked on the hERG channel from the extracellular side of the cell

membrane. The apparent slow onset of drug effects shown in Fig. 5A-C was due to the slow

superfusion rate in these experiments to conserve drugs.

We further tested whether the effects of PD and NS were related to each other in binding

site or mechanism of action. In these experiments, PD 20 uM was applied to the hERG channel

expressed in oocytes using direct pipetting. After PD effect stabilized, NS 30 uM was applied in

the continuous presence of PD. NS effects were compared with those measured in the absence of

PD. Fig. 5D shows that NS was equally effective in increasing hERG current without or with

PD, suggesting that the binding sites and mechanisms of action of these two hERG activators are

independent of each other.

4. **Cys substitutions introduced into the outer vestibule or the external pore entrance of**
    the hERG channel, or modifications of the engineered Cys side chains, differentially
    affected the activator actions of PD307243 and NS1643

Since both PD and NS worked from the extracellular side of the cell membrane and both

slowed the rate of hERG inactivation, our search for the drug binding sites targeted the outer

vestibule region and the pore entrance. It has been proposed that the hERG channel's inactivation

process is similar to the P-type inactivation described for the Shaker or Shaker-like channels

(Fan *et al.*, 1999; Lopez-Barneo *et al.*, 1993; Smith *et al.*, 1996). The P-type inactivation is

believed to arise from conformational changes around the outer mouth and in the pore-loop, that

alter ion selectivity or conductance of the selectivity filter and shut down K^+ ion flux through the

pore. Previously, we showed that the unusually long (~ 43 amino acids) extracellular S5-P linker

in the hERG channel also plays a critical role in the channel's inactivation process (Liu *et al*.,

2002). Mutations introduced into specific 'high-impact' positions along the S5-P linker can

disrupt the inactivation process (Dun *et al.*, 1999; Liu *et al*., 2002). The 4 S5- P linkers in a

tetrameric hERG channel, along with the P-S6 linkers, line the outer vestibule of the channel.

Since mutations along the S5-P linker that disrupted inactivation also impaired the hERG

channel's ability to select for K^+ ions (Dun *et al*., 1999; Liu *et al*., 2002), the linker must interact

with the pore loop in 3-D space. Indeed, our recent 3-D model for hERG's pore domain, based on

peptide toxin foot-printing experiments and homology modeling, suggested that side chains at

several 'high-impact' positions could make contact with pore-loop residues (Tseng *et al.*, 2007).

We have performed a detailed Cys-scanning mutagenesis study of the S5-P linker in the hERG

channel, and identified not only high-impact positions, but also 'intermediate-impact' positions

(Liu *et al*., 2002). Cys substitution *per se* at the intermediate-impact positions does not disrupt

the inactivation process or the pore's K^+ selectivity. However, modification of Cys side chains at

these positions markedly impacted on channel function. Furthermore, our data suggested that the

middle segment of the S5-P linker (positions 583 - 597) might adopt an α-helical structure. This

was confirmed by subsequent experiments using NMR spectroscopy (Jiang *et al.*, 2005; Torres *et

al.*, 2003). Interestingly, Cys side chains engineered into most positions along this 'S5-P helix'

could form intersubunit disulfide bonds (Jiang *et al*., 2005). We further showed that Cys side

chain introduced into position 584, 585, 588, and 589 on the S5-P helix could form intersubunit

disulfide bond with counterparts from adjacent subunits (Jiang *et al*., 2005). This may also be the

case for Cys side chain introduced into position 631 at the external pore entrance. In all cases,

disulfide bond formation disrupted the inactivation process and the K^+ selectivity.

We took advantage of the available information and mutant channels to address the following question: how do Cys side chains introduced into the S5-P linker and the pore entrance positions, or a modification of these engineered Cys side chains, impact on the activator effects of PD and NS? We selected eight Cys substituted mutants that covered the region of interest (diagrammed in Fig. 6A). In all cases, oocytes were treated with DTT to reduce spontaneously formed disulfide bonds. In cases when disulfide bonds were needed to create the mutant phenotype (G584C, H587C and S631C), oocytes were treated with H_2O_2 (0.3%) in conjunction with depolarizing pulses (or incubated in elevated $[K]_o$ 20 mM) to facilitate intersubunit disulfide bond formation. The mutant phenotype was identified by a lack of bell-shaped current-voltage relationships (as shown in Fig. 1D and 1H), due to a disruption of the inactivation process. Furthermore, tail currents recorded at -60 or -80 mV turned in the inward direction, due to a loss of K^+ selectivity (so that extracellular Na^+ ions carried inward tail currents at these voltages). To guard against artifacts due to interference from oocyte endogenous currents, we confirmed that (1) currents in DTT-treated oocytes that had been injected with cRNAs for the Cys-substituted mutants were significantly larger than currents in uninjected oocytes, and (2) PD at 20 uM had no noticeable effects on currents in uninjected oocytes (data not shown).

We quantified drug effects on current amplitudes through channels with the mutant phenotype from test pulse currents measured at +60 mV, the highest amounts of outward current in the voltage range tested. PD 20 uM or NS 30 uM was applied to the bath solution by direct pipetting. Drug effects were evaluated in a 'yes-or-no' fashion. We did not attempt to quantitatively compare the degrees of drugs' activator effects among the channels. Fig. 6B shows that PD was effective in increasing currents through all the channels in either the WT-like or the mutant mode. Therefore, conformational changes in the outer vestibule or the pore entrance did

not prevent the activator effect of PD. This is the case even with intersubunit disulfide bond

formation in G584C, H587C or S631C, which was expected to alter the peptide backbone

conformation and flexibility. On the other hand, although NS was effective in increasing currents

through the channels when they were in the WT-like gating mode, the drug could not induce the

activator effect when the channels were in the mutant mode (Fig. 6C).

Original data are shown in Figs. 6D and Fig. 7 to support the above conclusions. Fig. 6D

illustrates representative current traces recorded from G572C, G584C (disulfide bonded),

W585C, H587C (disulfide bonded), and N588C. NS 30 uM did not induce the activator effect

(and a modest current-suppressing effect on W585C was revealed). In the continuous presence of

NS, PD 20 uM effectively increased outward current at +60 mV as well as inward current at -120

mV. Fig. 7 illustrates the impact of modifying Cys side chains introduced into the external pore

entrance, T613C and S631C. Cys substitution *per se* (in the free thiol state) at these 2 positions

did not affect the channel function: they were WT-like in showing strong inactivation and K^+

selectivity. However, MTSET modification of T613C impaired the channel's ability to inactivate

or to select for K^+ ions (Fig. 7A). Treating S631C with 0.3% H_2O_2 while depolarizing the

membrane to cause channel activation and inactivation effectively converted the S631C channel

to the mutant phenotype: impaired inactivation and K^+ selectivity (Fig. 7B) (Fan *et al.*, 1999).

PD 20 uM effectively increased both outward currents and inward currents through the T613C

and S631C channels in both WT-like and mutant modes (left columns of Figs. 7C and 7D). On

the other hand, although NS 30 uM was effective in increasing currents through the two channels

when they were in the WT-like mode, it could not induce any activator effect when the channels

were in the mutant mode (right columns of Figs. 7C and 7D). Note that MTEST, DTT or H_2O_2

had no effect on the gating kinetics or K^+ selectivity of WT hERG (Fan *et al*., 1999). DTT or

H_2O_2 treatment did not impair the agonist effect of NS on WT hERG (data not shown).

5. **Using external and internal hERG pore blockers to further probe the sites for the**

    activator actions of PD307243 and NS1643

Previously, we showed that a scorpion peptide toxin, BeKm-1, binds to the outer

vestibule of the hERG channel to suppress its currents (Fig. 8A) (Zhang *et al*., 2003). We further

identified the following hERG residues that are likely to make direct contacts with the bound

BeKm-1 peptide: R582, I583, Y597 (at the two ends of the S5-P helix) and S631 (at the pore

entrance) (Tseng *et al*., 2007). We hypothesized that BeKm-1 binding might differentially

impact on the binding and/or action of PD and NS. Indeed, Figs. 8B - 8D show that BeKm-1

potentiated PD's activator effect while suppressed NS's activator effect.

Positively charged quaternary ammonium cations (QA^+) have been used as a tool to

probe the ion conduction pathway of K channels (Ahern *et al.*, 2006). In the Shaker or Shaker-

like channels, QA^+ applied from outside the cell membrane binds to the external pore entrance to

occlude currents through the pore. Although extracellular TEA has a low binding affinity to

hERG (50% reduction at ~ 50 mM) (Pardo-Lopez *et al.*, 2002), lengthening the hydrocarbon

chain length greatly increased the binding affinity, so that 50 uM tetrapentyl ammonium cation

($TPeA^+$) could suppress the current by $\geq 80\%$ (Fig. 9A). $TPeA^+$ effectively prevented the

activator effect of PD. Instead, $TPeA^+$ unmasked a concentration-dependent current suppressing

effect of PD (Fig. 9B).

Dofetilide binds to the hERG channel from the intracellular side of the cell membrane

(Kamiya *et al*., 2006). An Ala scanning mutagenesis approach has been used to probe the

dofetilide binding site in the hERG channel (Kamiya *et al*., 2006): Y652A, F656A on the S6

helix, T623A, S624A and V625A along the selectivity filter of the pore-loop, as well as G648

(on S6, juxtaposed to the pore-loop) greatly attenuated the dofetilide binding affinity. Therefore

the dofetilide binding site is likely formed with S6 helices and roofed by the pore-loop (cartoon

in Fig. 9C). Applying dofetilide 0.5 uM to hERG expressed in oocytes in conjunction with

constant pulsing to cause channel activation led to a gradual decrease in current amplitude,

reaching a suppression of $\geq$ 80% in 15-20 min (Fig. 9D). Under these conditions, dofetilide

effectively prevented the activator effect of PD, and unmasked its current suppressing effect.

Thus, although the PD's activator effect on the hERG channel could not be disrupted by

interventions applied to the extracellular S5-P linker or the external pore entrance, it was

prevented by blockers that could reduce K^+ ion occupancy in the selectivity filter of the hERG

channel (more in *Discussion*).

DISCUSSION

The major findings in this study can be summarized as the following. The concentration-

response relationships of PD and NS on the hERG channel could be described by a 1:1 binding

stoichiometry, with the maximal effect being 100% and $\geq$ 300% increase in the current

amplitude (measured as time-dependent current during 1-s step to 0 mV) with apparent K_d values

of 3 and 20 uM, respectively. The activator effect of PD was accompanied by a slowing of hERG

inactivation. On the other hand, the activator effect of NS involved not only a slowing of hERG

inactivation, but also an acceleration of channel activation as well as retardation of channel

deactivation. Both drugs worked on the hERG channel from the extracellular side of the cell

membrane. Inactivation-disrupting mutations or side chain modifications introduced into the

outer vestibule or pore entrance of the hERG channel abolished the activator effect of NS, but

did not prevent the activator effect of PD. BeKm-1, a peptide toxin that bound to the outer

vestibule of the hERG channel (Tseng *et al.*, 2007) greatly attenuated the activator effect of NS,

but potentiated the activator effect of PD. Finally, the activator effect of PD was prevented by an

external pore blocker, tetrapentylammonium (Ahern *et al.*, 2006), or by dofetilide that is known

to bind to the inner cavity of the hERG channel (Kamiya *et al.*, 2006).

1. Binding site and mechanism of action of NS1643

Our data support the notion that the NS binding site is formed by the outer vestibule and

pore entrance of the hERG channel. The positions where Cys substitution or side chain

modification abolished NS's activator effects (e.g. 572 at the extracellular end of S5, positions

along the S5-P helix between 584 and 593, 613 and 631 at the external pore entrance) may be

close to each other in 3-D space (Fig. S2 in *Supplemental Data*). Our previous studies suggested

that the S5-P helices in the hERG channel must be able to adopt dynamic conformational

changes during membrane depolarization, so that a considerable portion of their surfaces can

come close to each other to allow intersubunit disulfide bond formation between Cys side chains

at equivalent positions (Jiang *et al.*, 2005). Furthermore, our 3-D model of the hERG channel

pore domain suggested that W585 and L589 side chains on the S5-P helices can make contacts

with pore-loop side chains (Tseng *et al.*, 2007), providing an explanation for why mutations

along the S5-P linker can impact on the channel's K^+ selectivity (Tseng *et al.*, 2007).

It is not surprising that putative NS binding to a domain formed by the outer

vestibule/external pore entrance can influence the rates of activation and deactivation. These

gating processes are believed to occur at the cytoplasmic halves of the S6 segments, controlled

by the voltage-sensor S4 via the S4-S5 linkers (Long *et al.*, 2005). The extracellular end of S4 in

the activated state can come close to the extracellular end of S5 from an adjacent subunit (to

allow intersubunit disulfide bond formation) (Gandhi *et al.*, 2003; Laine *et al.*, 2003). Therefore,

drug binding to the outer vestibule/external pore entrance may allosterically affect the stability of

S4 segment in the activated state. Indeed, we have shown that Cys substitutions at high-impact

positions in the outer vestibule of the hERG channel could affect not only inactivation/K^+

selectivity, but also the voltage-dependence of activation (Liu *et al.*, 2002).

Our data are subject to alternative explanations. Data in Figs. 5 and 6 can be alternatively

explained by a removal of the mechanism for NS action. Data in Fig. 8 can be alternatively

explained by a reorientation of the channel upon BeKm-1 binding, preventing access to an NS

binding site in other area(s) of the channel.

2. **Binding site and mechanism of action of PD307243**

The activator effect of PD was very robust. PD remained effective even when

intersubunit disulfide bonds were formed between S5-P helices. Such intersubunit disulfide

bonds were expected to perturb the peptide backbone conformation and flexibility. However,

extracellularly applied TPeA and intracellularly-acting dofetilide prevented the activator effect of

PD. What are the common features shared by these two pore blockers that acted from the

opposite sides of the cell membrane? An X-crystallographic study has revealed the binding sites

for external TEA and internal tetrabutylammonium (TBA) and their effects on Tl^+ (a K^+ analog)

ion occupancy in the selectivity filter of the KscA channel (Lenaeus *et al.*, 2004). It is reasonable

to apply information learned from the crystallographic work on KcsA to our study for the

following reasons. First, it has been shown that the binding site and likely the mechanism of

action of extracellular quaternary ammonium (QA^+) cation are similar among different K

channels (Ahern *et al*., 2006). Second, although TBA and dofetilide are distinctly different

molecules, TBA binding to the KcsA channel and dofetilide binding to the hERG channel share

two important features: (1) they both bind deep in the channel inner cavity, right beneath and

likely making contact with the pore-loop, and (2) binding is stabilized by hydrophobic

interactions between the blockers and aromatic residues facing toward the inner cavity (F103 in

KcsA and the equivalent Y652 in hERG) (Kamiya *et al*., 2006; Lenaeus *et al*., 2004). External

TEA binding and internal TBA binding to the KcsA channel share two features: (1) the

selectivity filter becomes largely devoid of Tl^+ ions, and (2) the peptide backbone of the

selectivity filter exhibits subtle conformational changes (Lenaeus *et al*., 2004). While these

observations explain why external TEA and internal TBA (or external TPeA and internal

dofetilide, in the case of hERG) can totally occlude K^+ ion flux through the pore, they also

suggest that PD may be a 'pore modifier'.

To explain why PD is sensitive to the degree of K^+ ion occupancy in the selectivity filter,

we hypothesize that PD directly acts on the pore-loop to increase channel conductance and

secondarily/additionally retard hERG inactivation. Although we were able to qualitatively

simulate PD effects on the WT hERG channel by a 50% reduction in the inactivation rate,

introducing an increase in channel conductance in the parameter set might improve model

simulation quantitatively. Interventions that disrupted hERG inactivation did not prevent PD's

agonist effect. In these cases, PD might work by primarily increasing channel conductance,

although the interventions might have also affected PD binding affinity and/or degree of increase

in the channel conductance. To provide direct experimental evidence for the hypothesis, we need

to perform outside-out patch recordings of single channel currents through WT and inactivation-

disrupted channels under the control conditions and after the application of increasing

concentrations of PD. Such extensive experiments are beyond the scope of the current study.

BeKm-1 potentiated the activator effect of PD. What are the differences between TPeA

and BeKm-1, both of which bound to the outer mouth of the hERG channel? BeKm-1 differs

from TPeA in two aspects. First, the peptide toxin binds above the pore entrance, and does not

totally occlude K^+ ion flux through the pore (Tseng *et al.*, 2007; Zhang *et al.*, 2003). Second,

BeKm-1 binds to the hERG outer vestibule in the resting and activated states but unbinds in the

inactivated state, probably due to the dynamic conformational changes in this region discussed

above (Tseng *et al.*, 2007). Therefore, the extracellular BeKm-1 peptides may go through

binding and unbinding cycles under our voltage clamp conditions, and the presence of PD

through its pore-modifier effect may retard BeKm-1 binding or facilitate BeKm-1 unbinding,

producing an apparent potentiation of its activator effect.

3. Comparison with previous studies

Our results on NS1643 are consistent with a previous study (Casis *et al.*, 2006): pore

mutations that impair hERG inactivation (S631A, G628C/S631C and S620T) attenuate the

activator effect of NS. Our results on PD307243 are similar to a previous study on its structure

analog, PD118057 (Zhou *et al.*, 2005): PD118057 did not affect the voltage-dependence or

kinetics of activation and deactivation, and it slowed the rate of hERG inactivation at 35°C. A

recent report on PD307243 (1 - 10 uM, applied to the hERG channel stably expressed in CHO

cells) had some very novel findings (Gordon *et al.*, 2008). The authors showed that PD307243

not only increased the hERG current amplitude, but also created a prominent constitutive

component and greatly slowed the rate of channel inactivation. The combined effects of

constitutive channel activation and markedly slowed inactivation created a peculiar transient

outward (I_{to})-like current. We have not observed such a PD-induced I_{to}-like current or

constitutive channel activation in oocytes or COS-7 cells. We have confirmed the chemical

structure of PD307243 used in our experiments (*Supplemental Data*). Importantly, we have

confirmed the agonist effect of PD on native I_{Kr} in guinea pig ventricular myocytes (Fig. 10). In

3 separate experiments, 10 uM PD increased the time-dependent outward current recorded at -10

or -20 mV (mainly reflecting I_{Kr}) by 41, 95 and 193% after exposure times of 1.5, 4 and 7 min,

respectively. PD did not induce any I_{to}-like current in guinea pig ventricular myocytes.

ACKNOWLEDGEMENTS

REFERENCES

Ahern CA, Eastwood AL, Lester HA, Dougherty DA, and Horn R. (2006) A cation-π interaction between extracellular TEA and an aromatic residue in potassium channels. J Gen Physiol **128**:649-657.

Brugada R, Hong K, Dumaine R, Cordeiro JM, Gaita F, Borggrefe M, Menendez TM, Brugada J, Pollevick GD, Wolpert C, Burashnikov E, Matsuo K, Wu YS, Guerchicoff A, Bianchi F, Giustetto C, Schimpf R, Brugada P, and Antzelevitch C. (2004) Sudden death associated with short-QT syndrome linked to mutations in HERG. Circulation **109**:30-35.

Casis O, Olesen S-P, and Sanguinetti MC. (2006) Mechanism of action of a novel human ether-a-go-go-related gene channel activator. Mol Pharm **69**:658-665.

Dun W, Jiang M, and Tseng G-N. (1999) Allosteric effects of mutations in the extracellular S5-P loop on the gating and ion permeation properties of *hERG*. Pflugers Archiv **439**:141-149.

Fan J-S, Jiang M, Dun W, McDonald TV, and Tseng G-N. (1999) Effects of outer mouth mutations on *hERG* channel function: a comparison with similar mutations in *Shaker*. Biophys J **76**:3128-3140.

Gandhi CS, Clark E, Loots E, Pralle A, and Isacoff EY. (2003) The orientation and molecular movement of a K^+ channel voltage-sensing domain. Neuron **40**:515-525.

Gordon E, Lozinskaya IM, Lin Z, Seus SF, Blaney FE, Willette RN, and Xu X. (2008) 2-[2-(3,4-dichloro-phenyl)-2,3-dihydro-1H-isoindol-5-ylamino]-nicotinic acid (PD-307243) causes instantaneous current through human ether-a-go-go-related gene potassium channels. Mol Pharm 73;639-651.

Hansen RS, Diness TG, Christ T, Demnitz J, Ravens U, Olesen S-P, and Grunnet M. (2006) Activation of human ether-a-go-go-related gene potassium channels by the diphenylurea 1,3-bis-(2-hydroxy-5-trifluoromethy-phenyl)-urea (NS1643). Mol Pharm **69**:266-277.

Jiang M, Zhang M, Maslennikov IV, Liu J, Wu DM, Korolkova YV, Arseniev AS, Grishin EV, and Tseng G-N. (2005) Dynamic conformational changes of extracellular S5-P linkers in the hERG channel. J Physiol **569**:75-89.

Kamiya K, Niwa R, Mitcheson JS, and Sanguinetti MC. (2006) Molecular determinants of hERG channel block. Mol Pharm **69**:1709-1716.

Kang J, Chen X-L, Wang H, Ji J, Cheng H, Incardona J, Reynolds W, Viviani F, Tabart M, and Rampe D. (2005) Discovery of a small molecule activator of the human ether-a-go-go-related gene (HERG) cardiac K$^+$ channel. Mol Pharm **67**:827-836.

Laine M, Lin M-CA, Bannister JPA, Silverman WR, Mock AF, Roux B, and Papazian DM. (2003) Atomic proximity between S4 segment and pore domain in Shaker potassium channels. Neuron **39**:467-481.

Lenaeus MJ, Vamvouka M, Focia PJ, and Gross A. (2004) Structural basis of TEA blockade in a model potassium channel. Nature Structural & Molecular Biology **12**:454-459.

Liu J, Zhang M, Jiang M, and Tseng G-N. (2002) Structural and functional role of the extracellular S5-P linker in the HERG potassium channel. J Gen Physiol **120**:723-737.

Long SB, Campbell EB, and MacKinnon R. (2005) Voltage sensor of Kv1.2: structural basis of electromechanical coupling. Science **309**:903-908.

Lopez-Barneo J, Hoshi T, Heinemann SH, and Aldrich RW. (1993) Effects of external cations and mutations in the pore region on C-type inactivation of Shaker potassium channels. Receptors and channels **1**:61-71.

Pardo-Lopez L, Zhang M, Liu J, Jiang M, Possani LD, and Tseng G-N. (2002) Mapping the binding site of a HERG-specific peptide toxin (ErgTx) to the channel's outer vestibule. J Biol Chem **277**:16403-16411.

Perry M, Saches FB, and Sanguinetti MC. (2007) Structural basis of action of a human ether-a-go-go-related gene 1 potassium channel activator. PNAS **104**:13827-13832.

Recanatini M, Poluzzi E, Masetti M, Cavalli A, and De Ponti F. (2005) QT prolongation through hERG K^+ channel blockade: current knowledge and strategies for the early prediction during drug development. Med Res Rev **25**:133-166.

Roden DM. (2004) Drug-induced prolongation of the QT interval. New England Journal of Medicine **350**:1013-1022.

Sanguinetti MC, Jiang C, Curran ME, and Keating MT. (1995) A mechanistic link between an inherited and an acquired cardiac arrhythmia: HERG encodes the I_{Kr} potassium channel. Cell, **81**:299-307.

Sanguinetti MC and Jurkiewicz NK. (1990) Two components of cardiac delayed rectifier K^+ current. Differential sensitivity to block by class III antiarrhythmic agents. J Gen Physiol **96**:195-215.

Schreibmayer W, Lester HA, and Dascal N. (1994) Voltage clamping of Xenopus laevis oocytes utilizing agarose-cushion electrodes. Pflugers Archiv **426**:453-458.

Smith PL, Baukrowitz T, and Yellen G. (1996) The inward rectification mechanism of the HERG cardiac potassium channel. Nature **379**:833-836.

Torres AM, Bansal P, Sunde M, Clarke CE, Bursill JA, Smith DJ, Bauskin A, Breit SN, Campbell TJ, Alewood PF, Kuchel PW, and Vandenberg JI. (2003) Structure of the HERG K^+ channel S5P extracellular linker: role of an amphipathic α-helix in C-type inactivation. J Biol Chem **278**:42136-42148.

Tseng G-N. (2001) I$_{Kr}$: the hERG channel. J Mol Cell Cardiol **33**:835-849.

Tseng G-N, Sonawane KD, Korolkova YV, Zhang M, Liu J, Grishin E, and Guy HR. (2007)
Probing outer mouth structure of the hERG channel with peptide toxin foot printing and
molecular modeling. Biophys J **92**:3524-3540.

Wang S, Liu S, Morales MJ, Strauss HC, and Rasmusson RL. (1997) A quantitative analysis of
the activation and inactivation kinetics of *HERG* expressed in *Xenopus* oocytes. J Physiol
502:45-60.

Yao J-A, Jiang M, Fan J-S, Zhou Y-Y, and Tseng G-N. (1999) Heterogeneous changes in K
currents in rat ventricles three days after myocardial infarction. Cardiov Res **44**:132-145.

Yeola SW, Rich TC, Uebele VN, Tamkun MM, and Snyders DJ. (1996) Molecular analysis of a
binding site for quinidine in a human cardiac delayed rectifier K$^+$ channel. Role of S6 in
antiarrhythmic drug binding. Circ Res **78**:1105-1114.

Zhang H, Zhu B, Yao J-A, and Tseng G-N. (1998) Differential effects of S6 mutations on
binding of quinidine and 4-aminopyridine to rKv1.4: common site but different factors in
determining blockers' binding affinity. J Pharm Exp Ther **287**:332-343.

Zhang M, Korolkova YV, Liu J, Jiang M, Grishin EV, and Tseng G-N. (2003) BeKm-1 is a hERG-specific toxin that shares the structure with ChTx but the mechanism of action with ErgTx1. Biophys J **84**:3022-3036.

Zhou J, Augelli-Szafran CE, Bradley JA, Chen X, Koci BJ, Volberg WA, Sun Z, and Cordes JS. (2005) Novel potent human ether-a-go-go-related gene (hERG) potassium channel enhancers and their in vitro antiarrhythmic activity. Mol Pharm **68**:876-884.

Footnote to the title:

This study was supported by RO1 HL46451 and HL67840 (GNT) from the National Heart, Lung

and Blood Institute of National Institutes of Health.

LEGENDS FOR FIGURES

Scheme legend: R and R* represent fractions of channels in activator-free and activator-bound states, D is activator drug, K_{on} and K_{off} are binding and unbinding rate constants, and K_d is dissociation constant.

Fig. 1 Characterization of the effects of PD 307243 (PD) on the hERG channel expressed in oocytes. (A) *Upper*: Superimposed hERG current traces before (black) and after PD application (1, 2, 5, 10, 20, and 50 uM, traces shown in the same colors as those of symbols in the lower panel). The currents were elicited by the voltage clamp protocol diagrammed on top applied once every min. *Lower*: Time course of changes in hERG current amplitude from the same experiment. Current amplitudes were measured from the time-dependent current during the 0 mV step and normalized by the control current right before the start of PD application. **(B)** Concentration-response relationship. Numbers of measurements are shown in parentheses. The superimposed curve was calculated from equation [1] (see text), with 'fold increase in current amplitude' (parameter 'A' in equation [1]) = 2, and apparent dissociation constant K_d = 3 uM. In the following panels, data points and current traces recorded under the control conditions are shown in black, and those recorded in the presence of PD (10 uM) are shown in red. **(C)** PD did not shift the 1-s isochronal activation curve of hERG. *Inset*: voltage clamp protocol and representative current traces. The relationship between V_t and peak amplitude of tail current (I_{tail}) was fit with a Boltzmann function: $I_{tail} = I_{max}/[1+exp(V_{0.5}-V_t)/k]$, to estimate the maximal peak tail current amplitude (I_{max}), half-maximal activation voltage ($V_{0.5}$) and slope factor (k). I_{tail} was normalized by I_{max} (I_{tail}/I_{max} = fraction activated) and plotted against V_t. **(D)** PD increased hERG test pulse currents in a voltage-dependent manner. The voltage clamp protocol was the same as that described for panel (C). For each oocyte, amplitudes of time-dependent currents during 1-s

test pulses to V_t were normalized by the control current at V_t -10 mV. The current ratios, I_d/I_c, are also plotted based on the right coordinate. **(E)** PD did not alter the time course of hERG activation. *Inset*: 'envelope' voltage clamp protocol and representative current traces. The rate of hERG activation was slower than inactivation. Thus the time course of activation could not be directly measured from the test pulse currents. Since the outward tail currents signified channels recovered from inactivation, the time course of growth of peak tail current amplitude after increasing durations of depolarizing pulses could be used to infer the time course of channel activation. The membrane voltage was stepped to V_t for durations varying from 5 to 1000 ms in 50 ms increments. The time course of growth of peak tail current amplitude was fit with a single exponential function to generate $\tau_{activation}$ (plotted on a logarithmic scale so that the slope indicates the voltage-sensitivity of the underlying gating process). **(F)** PD did not alter the time course of hERG deactivation. *Inset*: voltage clamp protocol. Tail currents during 2- to 5-s step to V_r were fit with a double exponential function to generate the fast and slow time constants of deactivation (τ_{fast} and τ_{slow}, right and left coordinates, respectively). In V_r range $\leq$ -100 mV, channel deactivation was almost exclusively the fast component; thus τ_{slow} values are not shown. **(G)** PD modestly slowed the rate of hERG inactivation. *Inset*: triple-pulse voltage clamp protocol and representative current traces during the third step (indicated by gray shade in the protocol diagram). The blue trace represents control current trace scaled to match the amplitude of current in PD. hERG inactivation was faster than activation. To bypass the slow activation process, the hERG channels were first fully activated and inactivated by a 1-s step to +60 mV. This was followed by a brief 15-ms step to -80 mV during which the channels recovered from inactivation without appreciable deactivation. The third depolarizing step to various V_t caused channel transition from open to inactivated states. The decay of current traces during the third pulse was

fit with a single exponential function to generate time constant of inactivation ($\tau_{inactivation}$). The
rate of inactivation (reciprocal of $\tau_{inactivation}$, left coordinate, logarithmic scale) was plotted against
V_t. The relationship between the rate of inactivation and V_t in the range of 0 to +60 mV was fit
with equation [2]: $K(V_t) = K(0)\exp(z_{ina}V_tF/RT)$, where $K(V_t)$ and $K(0)$ are rates of inactivation
at V_t and 0 mV, respectively, z_{ina} is equivalent gating charge of inactivation, F, R and T are
Faraday constant, gas constant and absolute temperature, respectively. The lines superimposed
on the data points were calculated from equation [2], with K(0) and z_{ina} values of 0.23 ms^{-1} and
0.72 for control, 0.12 ms^{-1} and 0.71 for PD. * $p < 0.05$, PD vs control. **(H)** PD increased both
outward and inward currents through the hERG channel. The voltage clamp protocol was the
same as that diagrammed in (F). For each cell, current amplitudes were measured from the peak
or plateau level of tail currents (defined as fully-activated current, or I_{f-a}) and normalized by the
control I_{f-a} at -50 mV.

Fig. 2 Characterization of the effects of NS 1643 (NS) on the hERG channel expressed in
oocytes. Voltage clamp protocols and methods of data analysis are the same as those described
for corresponding panels in Fig. 1. [NS] for experiments shown in panels (C)-(H) was 30 uM.
(A) Time course of changes in hERG current amplitude before and during exposure to NS at the
specified concentrations. **(B)** Concentration-response relationship. The superimposed curve was
calculated from equation [1] with 'fold increase in current amplitude' = 3.24, K_d = 20 uM.**(C)** NS
shifted the 1-s isochronal activation curve of hERG in the negative direction by -9.8 ± 1.4 mV (n
= 7). **(D)** NS increased hERG test pulse current in a voltage-dependent manner. **(E)** NS
accelerated hERG activation (shortened $\tau_{activation}$). **(F)** NS slowed hERG deactivation, manifested
as a prolongation of τ_{fast} and τ_{slow}. **(G)** NS slowed hERG inactivation. The lines superimposed on

the data points were calculated from equation [2] (described for Fig. 1G), with values of K(0)

and z_{ina} 0.02 ms^{-1} and 0.6 for control, 0.01 ms^{-1} and 0.5 for PD. **(H)** NS increased both outward

and inward currents through the hERG channel. * $p < 0.05$, NS vs control.

Fig. 3 Model simulation of the effects of PD307243 (A) and NS1643 (B) on the hERG

channel. The model and parameter values are listed in Table1. Simulated current traces and data

points for control, PD and NS are shown in black, red and blue, respectively. For each column,

'a' and 'd' show superimposed simulated current traces elicited by the voltage clamp protocols

diagrammed in the insets (time scale was the same as protocols shown in Fig. 1), 'b' depicts

simulated 1-s isochronal activation curves, and 'c' illustrates simulated test pulse current-voltage

relationship (open symbols, left coordinate) and current ratio (I_d/I_c, right coordinate). Inset of

panel Aa shows horizontally shifted inward tail currents at -120 mV, to illustrate the difference

in the peak current amplitude.

Fig. 4 Concentration-response relationships of PD307243 (A) and NS1643 (B) on hERG

current amplitude and gating kinetics. ΔAMP: % increase in current amplitude measured as

time-dependent current during 1-s step to 0 mV. $\Delta V_{0.5}$: shift in $V_{0.5}$ of activation. $\Delta Rate_{INAC}$: %

decrease in rate of channel inactivation at 0 mV. Data were averaged from 4 - 6 measurements

each.

Fig. 5 Both PD307243 and NS1643 worked from outside the cell membrane yet their effects

were independent of each other. **(A)** *Left*: Time course of changes in hERG current amplitude

expressed in a COS-7 cell before, during, and after bath application of PD (PD_o, 10 uM), and

total current suppression by dofetilide (DOF). Currents were elicited by the voltage clamp

protocol diagrammed on top of the right panel. Current amplitudes were measured from the peak

of tail current at -60 mV and normalized by the control right before PD application. The time

course of onset of PD effect was fit with a single exponential function with τ value of 6 min.

Right: superimposed current traces from the same experiment at time points 'a', 'b' and 'c'. **(B)**

and **(C)** *Left*: Time courses of changes in hERG current amplitude expressed in oocytes before

and after intra-oocyte drug injection (estimated cytoplasmic concentrations denoted: $PD_i \sim 300$

uM and $NS_i \sim 1000$ uM), during exposure to drugs applied to the bath solution (PD_o 10 uM, NS_o

30 uM) and after intra-oocyte injection of TEA ($TEA_i \sim 2$ mM). In each experiment, the same

injecting pipette was used first for PD or NS injection and then for TEA injection. *Right*:

Superimposed current traces from the same experiments as in left panels at the specified time

points. *Inset* of right panel in (B): % increase in hERG current amplitude caused by 10 uM PD

tested in COS-7 cells and in oocytes measured from the peak amplitudes of outward tail currents

at -60 mV (66 ± 10 and 61 ± 8, n = 4 and 20, p > 0.05). The same conclusion could be reached by

measuring time-dependent test pulse currents at +40 mV: PD increased the current by $187\pm67\%$

and $185\pm16\%$ in COS-7 cells and in oocytes, respectively. **(D)** *Left*: Time course of changes in

hERG current amplitude before and during bath application of 20 uM PD and after adding NS 30

uM in the continuous presence of PD. *Right*: % increase in current amplitude caused by NS in

the absence or presence of PD ('-' and '+' PD).

Fig. 6 Summary of effects of Cys substitution or Cys side chain modification introduced

into the outer vestibule or pore entrance of the hERG channel on the activator action of

PD307243 and NS1643. (A) *Top*: 2-D diagram of a hERG subunit, marking S1 - S6

transmembrane helices, pore-loop, and the extracellular S5-P helix. *Lower*: amino acid sequence

of the S5-P linker, marking the positions that participate in forming the S5-P helix. High- and

intermediate-impact positions are highlighted by white letterings on black shade and by gray

shade, respectively. The positions examined in Figs. 6 and 7 are noted below the sequence. T613

and S631 are marked in the 2-D diagram. **(B)** and **(C)** Percent change in current amplitude

measured at 0 mV (WT or WT-like) or +60 mV (mutant) induced by 20 uM PD or 30 uM NS

plotted against the channel types along the abscissa in (C), where Cys side chains modified by

disulfide bonding (-S-S-) or MTSET modification (+MTS) are noted. Hatched histogram bars for

WT or WT-like channel phenotype are shown in white background, while those for mutant

phenotype are shown in black background (*inset* in 'C'). **(D)** Superimposed current traces

recorded from oocytes expressing the specified hERG mutants. Currents were elicited by the

voltage clamp protocol diagrammed on top under 3 conditions: control (light gray traces), after

adding 30 uM NS (dark gray traces), and after adding 20 uM PD in the continuous presence of

NS (black traces).

**Fig. 7 Modifications of Cys side chains introduced into 2 pore entrance positions
differentially impacted on the 'activator' effects of PD307243 and NS1643.** *C*urrents were

elicited by different voltage clamp protocols to (a) illustrate their gating behavior as WT-like or

Mutant, and (b) probe for drug effects on both outward and inward currents through the

channels. For the sake of simplicity, individual voltage clamp protocols are not shown; only the

step voltages are noted (holding voltage was -80 mV in all cases). **(A)** T613C manifested WT-

like gating behavior under the control conditions (gray trace), and switched to the mutant

behavior after MTSET modification (black trace). **(B)** S631C manifested WT-like behavior (gray

trace) when DTT treated, but switched to Mutant behavior (black trace) after H_2O_2 treatment

with pulsing. **(C)** and **(D)** PD was effective in increasing currents through the T613C and S631C

channels in both WT-like and mutant behavior. On the other hand, NS was effective in

increasing currents through the T613C and S631C channels in the WT-like mode, but incapable

of increasing currents when the channels were in the mutant mode.

Fig. 8 BeKm-1 potentiated the activator effect of PD307243 but suppressed the activator

effect of NS1643. (A) Cartoon of hERG pore domain with an extracellular BeKm-1 structure.

Three hERG subunits are depicted, with the fourth one closest to viewers removed to reveal the

narrow selectivity filter and wide inner cavity of the pore. Cylinders represent the S5-P helices.

(B) *Main plot*: Two time courses of changes in hERG current amplitude before and after

exposure to PD 20 uM. Current amplitudes were measured from time-dependent currents during

1-s steps to 0 mV and normalized by the current right before PD application. One experiment

(open symbols) was conducted in the absence of BeKm-1. The other (black symbols) was

conducted in the presence of 10 uM BeKm-1. *Inset*: The complete time course of the second

experiment: BeKm-1 suppressed the current by 80% and subsequent application of PD in the

continuous presence of BeKm-1 effectively increased the current amplitude. **(C)** NS (30 uM)

effect on hERG in the absence or presence of BeKm-1. The format is the same as that of (B). **(D)**

Data summary. * $p < 0.05$, data obtained in the presence of BeKm-1 vs those without BeKm-1.

Fig. 9 An outer pore blocker, tetrapentylammonium cation (TPeA[+]) or an inner cavity

blocker, dofetilide (DOF) prevented the activator effect of PD307243 on hERG. (A) Cartoon

of a TPeA[+] ion binding to the outer pore entrance of hERG. **(B)** Time course of changes in

hERG current amplitude before and after application of 50 uM TPeA$^+$, and after application of

increasing concentrations of PD in the continuous presence of TPeA$^+$. Current amplitudes were

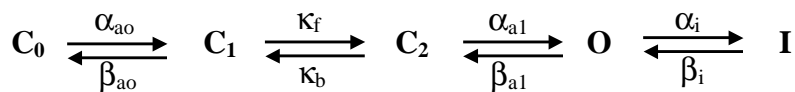measured from time-dependent currents during 1-s step to 0 mV and normalized by control.

Inset: Summary of PD (20 uM)-induced changes in hERG current amplitude in the absence or

presence of TPeA$^+$. **(C)** and **(D)** The format is the same as that in (A) and (B). DOF binds from

the intracellular side of the membrane to the inner cavity.

Fig. 10 Agonist effect of PD307243 on native I$_{Kr}$ in a guinea pig ventricular myocyte. Shown

are superimposed current traces recorded from the same myocyte before (thin gray trace) and 5

min after application of PD 10 uM (thick black trace). Currents were elicited by the pulse

protocol diagrammed**.** Based on the difference in voltage-dependence of activation (Sanguinetti

and Jurkiewicz1990), time-dependent current during the -10 mV step and the following tail

current at -50 mV mainly represented I$_{Kr}$. Time-dependent current during the +50 mV step

mainly represented I$_{Ks}$ although the following tail current resulted from both I$_{Kr}$ and I$_{Ks}$.

Table 1 Parameter values used in kinetic model[a] simulation of the effects of PD(307243) and NS(1643) on the hERG channel

Parameter	Unit	Control	PD[b]	NS[c]
$\alpha_{ao}(0)$	s^{-1}	22.3	22.3	22.3
z_{ao}		0.294	0.294	0.294
$\beta_{oa}(0)$	s^{-1}	0.047	0.047	0.047
z_{bo}		-1.577	-1.577	-1.577
κ_f	s^{-1}	23.8	23.8	23.8
κ_b	s^{-1}	36.8	36.8	36.8
$\alpha_{a1}(0)$	s^{-1}	13.7	13.7	**54.9**
z_{a1}		0.955	0.955	0.955
$\beta_{a1}(0)$	s^{-1}	0.069	0.069	**0.017**
z_{b1}		-1.045	-1.045	-1.045
$\alpha_i(0)$	s^{-1}	90.8	**45.4**	**45.4**
z_{ai}		0.585	0.585	0.585
$\beta_i(0)$	s^{-1}	6.5	6.5	6.5
z_{bi}		-0.817	-0.817	-0.817

a. The kinetic model of hERG gating was based on that of Wang et al (1997):

$$C_0 \underset{\beta_{ao}}{\overset{\alpha_{ao}}{\rightleftarrows}} C_1 \underset{\kappa_b}{\overset{\kappa_f}{\rightleftarrows}} C_2 \underset{\beta_{a1}}{\overset{\alpha_{a1}}{\rightleftarrows}} O \underset{\beta_i}{\overset{\alpha_i}{\rightleftarrows}} I$$

where C_x, O, and I represent closed states, open state and inactivated state, respectively. The

transitions between C_o and C_1, C_2 and O, as well as O and I are voltage-dependent, with rate
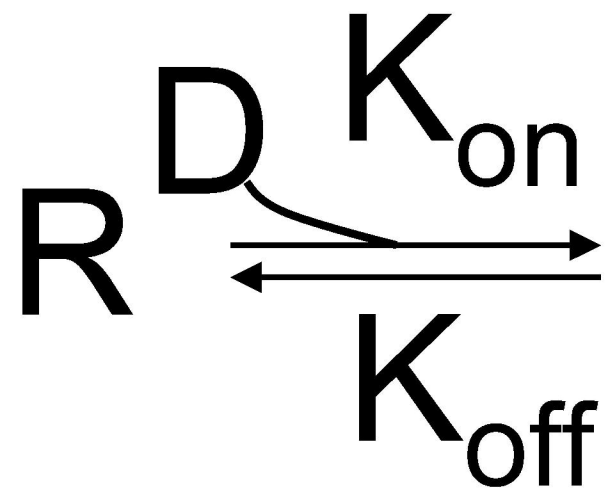
constants calculated as shown below:

$$\alpha_{a0}(V) = \alpha_{ao}(0)*\exp(z_{ao}VF/RT) \qquad \beta_{a0}(V) = \beta_{ao}(0)*\exp(z_{bo}VF/RT)$$

$$\alpha_{a1}(V) = \alpha_{a1}(0)*\exp(z_{a1}VF/RT) \qquad \beta_{a1}(V) = \beta_{a1}(0)*\exp(z_{b1}VF/RT)$$

$$\alpha_{i}(V) = \alpha_{i}(0)*\exp(z_{ai}VF/RT) \qquad \beta_{i}(V) = \beta_{i}(0)*\exp(z_{bi}VF/RT)$$

where $\alpha_x(V)$ and $\alpha_x(0)$ are forward (or right-ward according to the model) rate constants at

voltages of 'V' and 0 mV, respectively, and z_{ax} is the equivalent gating charge involved in the

gating transition; $\beta_x(V)$, $\beta_x(0)$ and z_{bx} are the corresponding parameters for the backward or left-

ward transitions. The transition between C_1 and C_2 is voltage-independent, with forward and

backward rate constants of κ_f and κ_b respectively.

b. The only change in parameter values for PD simulation was a 50% reduction in the 'O' to 'I'

transition rate (highlighted in **bold**).

c. The changes in parameter values for NS simulation included: 50% reduction in the 'O' to 'I'

transition rate, a 4-fold increase in the 'C_2' to 'O' transition rate, and a 75% reduction in 'O' to 'C_2'

transition rate (highlighted in **bold**).

$$R \underset{K_{off}}{\overset{D \quad K_{on}}{\rightleftharpoons}} R^* \quad K_d = K_{on}/K_{off}$$

Fig. 1

Fig. 2

A PD vs Control

a

b

Fraction activated

c

Test pulse current (normalized)

I_c
I_d
I_d/I_c

d

+60

0

-80

B NS vs Control

a

b

c

I_c
I_d
I_d/I_c

I_d/I_c

d

Fig. 3

Fig. 4

A PD$_o$ 10 uM   DOF 1 uM

τ = 6 min

hERG WT in COS-7

+40 / −60 / −80

b
a
c

B PD$_i$ (300 uM)

PD$_o$ 10 uM   TEA$_i$

τ = 2.3 min

hERG WT in oocyte

% increase by PD 10 uM

COS-7   Oocyte

b
a
c

C NS$_i$ (1000 uM)

NS$_o$ 30 uM   TEA$_i$

τ = 3.3 min

hERG WT in oocyte

b
a
c

D PD 20 μM

NS 30 μM

NS (30 μM)-induced increase in current (%)

PD   −   +

Fig. 5

Fig. 6

PD 20 μM   NS 30 μM

Control   After Drug

A

T613C

+60   -80

Control

MTSET
-treated

B

S631C

+60   -80

DTT

H₂O₂

C

T613C
Control
(WT)

+20   -60   -120

T613C
MTSET-
treated
(MUT)

+60   +20   -120

D

S631C
DTT-treated
(WT)

+40   -80

S631C
H₂O₂-treated
(MUT)

+40   -120

Fig. 7

A

BeKm-1

hERG outer vestibule

D

% increase (over control)

BeKm-1   -   +   -   +

PD   NS

B

Current (normalized)

BeKm-1   PD

in BeKm-1

no BeKm-1

C

BeKm-1   NS

no BeKm-1

in BeKm-1

Time after adding hERG activator (min)

Fig. 8

A TPeA$^+$

B

TPeA$^+$
(50 µM)

[PD] (µM)
1   2   5   10   20   50

TPeA$^+$ -   +

PD-induced $\Delta I_{0\,mV}$ (%)

Normalized current

0   30   60

C DOF

D

DOF
(0.5 µM)

1   2   5   10   20   50   [PD] (µM)

DOF   -   +

PD-induced $\Delta I_{0\,mV}$ (%)

Normalized current

0   30   60   min

Fig. 9

Guinea pig ventricular myocyte

$$I_{Kr} > I_{Ks} \qquad I_{Ks} > I_{Kr}$$

Control — PD 10 μM

200 pA

2 s

Fig. 10